

## Biodegradation of AZ31 and WE43 Magnesium Alloys in Simulated Body Fluid

Li Jiang<sup>1,2,\*</sup>, Fang Xu<sup>2</sup>, Zhen Xu<sup>1</sup>, Yu Chen<sup>1,3</sup>, Xuehua Zhou<sup>4</sup>, Guoying Wei<sup>2</sup>, Hongliang Ge<sup>2</sup>

<sup>1</sup>Department of Chemistry, Zhejiang University, Hangzhou 310027, China;

<sup>2</sup>College of Materials Science and Engineering, China Jiliang University, Hangzhou 310018, China;

<sup>3</sup>Department of Materials Science and Engineering, Zhejiang University, Hangzhou 310027, China;

<sup>4</sup>Shanghai Institute of Microsystem and Information Technology, Chinese Academy of Sciences, Shanghai 200050, China.

\*E-mail: [jiangliw@126.com](mailto:jiangliw@126.com)

Received: 11 September 2015 / Accepted: 13 October 2015 / Published: 4 November 2015

---

Biodegradation behavior and mechanism of AZ31 and WE43 magnesium alloys have been studied in the simulated body fluid (SBF). The results of weight loss tests indicate that corrosion rates of AZ31 alloy are lower than that of WE43 alloy. The corrosion resistance of magnesium alloys has a direct relationship with the alloying elements and microstructure. Corrosion processes of these two alloys are analyzed by electrochemical techniques. Over time corrosion potentials of AZ31 alloy and WE43 alloy both positively shift and corrosion rates decrease. Compared with WE43 alloy, corrosion current densities of AZ31 alloy are lower and the corrosion interface is relatively neat with a few shallow and narrow pits. Ascribed to serious local corrosion, the interface between corrosion products and matrix of WE43 alloy is sinuate with MgO<sub>4</sub>, MgCl<sub>2</sub> and Y<sub>2</sub>O<sub>3</sub> as part component of corrosion products.

---

**Keywords:** Magnesium alloy; Corrosion; Simulated body fluid

### 1. INTRODUCTION

For preferable mechanical property and excellent compatibility with human bone, magnesium alloy is present proposed as a promising biomaterial for the human body implant [1]. In the degradation process, magnesium alloy can offer the possibility of better physiological repair and better reconstruction of vascular compliance with minimum inflammatory response [2]. Nowadays, commercial alloys (AZ series and WE series magnesium alloys) are mostly under investigation as implant materials. AZ series magnesium alloys are usually alloyed with aluminum and zinc to improve corrosion resistance [3,4]. Aluminum is the most important alloying element and can significantly

improve tensile strength by forming  $Mg_{17}Al_{12}$  phase [5]. According to previous studies[2,6,7], AZ31 alloy is probably the most widely used commercial magnesium alloy and has better corrosion resistance among AZ series system[8-10]. WE series alloy is a kind of Al-free magnesium alloy. Some rare earth (RE) elements (Dy, Y, Nd and Gd) with acceptable toxicity are beneficial to enhance the mechanical and corrosion properties [11]. Due to excellent properties, e.g. relatively slow degradation in aqueous solutions and good electrochemical properties accompanied by excellent mechanical properties, WE43 alloy is suggested to be a suitable candidate for implant application material [12,13].

The two series magnesium alloys have different corrosion characteristics due to the different elements (Al or RE) contained, and embody their biodegradable superiority in some application aspects [3-13]. However, the comparison of effects of Al or RE elements in magnesium alloys on the degradation regularities in the same vitro study environments has been rare studied, and the difference of their degradation mechanism also has no clear conclusion [14]. In this paper, biodegradable processes of AZ31 alloy (Al element contained, RE elements free) and WE43 alloy (RE elements contained, Al element free) in simulated body fluid (SBF) has been studied, and the difference of their biodegradation mechanisms are revealed comprehensively. Gain a greater understanding of the difference of detailed degradation process and mechanism of magnesium alloy (Al/RE elements contained or free) can not only provide foundation of research in magnesium alloy contained Al and RE elements, but also direct the future composition design of the biodegradable magnesium alloy systems[15].

## 2. MATERIALS AND METHODS

### 2.1 Weight loss tests

The as-cast AZ31 alloy and extruded WE43 alloy are provided by Shanghai Institute of Microsystem and Information Technology, Chinese Academy of Sciences, Shanghai, China. The compositions of these two alloys are shown in table 1. Each sample (size: 12 mm × 12 mm × 10 mm) are hung with nylon line below the water surface 50 mm. The containers are 1000 mL beakers with 800 mL solution. The weight loss tests were conducted in quiescent solution for 30 days at room temperature (22~25°C). Simulated body fluid (SBF) is an aqueous solution which simulated the ion concentration of human blood without larger particles (proteins, lipids or blood cells). The composition of SBF is presented in table 2 with pH value of 7.4 and temperature 37°C [13].

**Table 1.** Composition of as-cast AZ31 alloy and extruded WE43 alloy

Element Concentration (wt.%)	Mg	Y	RE	Al	Zr	Zn	Mn	Si	Cu
AZ31 alloy	95.90	--	--	3.1	--	0.73	0.24	0.02	<0.001
WE43 alloy	91.35	4.16	3.80	--	0.36	0.20	0.13	--	--

**Table 2.** Composition of simulated body fluid[13]

Component	NaCl	CaCl <sub>2</sub>	KCl	MgSO <sub>4</sub>	NaHCO <sub>3</sub>	NaHPO <sub>4</sub>	NaH <sub>2</sub> PO <sub>4</sub>
Concentration(g/L)	6.800	0.200	0.400	0.100	2.200	0.126	0.026

According to ASTM-G31-72[16], the corrosion rate is calculated by the following equation:

$$\text{Corrosion rate} = (K \times W) / (A \times t \times D) \quad (1)$$

where the coefficient  $K = 8.76 \times 10^4$ ,  $W$  is the weight lost (g) before immersion and after cleaning the corrosion product,  $A$  is the sample area exposed to the solution (cm<sup>2</sup>),  $t$  is the exposure time (h) and  $D$  is the density of the material (g/cm<sup>3</sup>). After each immersion test, each sample are washed with double distilled water, dried with a blower and immersed in the chromic acid cleaning solution containing of 220g/L CrO<sub>3</sub> + AgNO<sub>3</sub> at room temperature for 5~10min to remove the corrosion products clearly [13].

## 2.2 Electrochemical test

Working electrodes are mounted in epoxy resin and exposed surface of 14×14 mm. They are grounded successively with 400~1200 grit SiC paper, washed with distilled water and dried by a blower. Potentialdynamic polarization curve and electrochemical impedance spectroscopy (EIS) measurement are performed on electrochemical working station (PARSTAT<sup>®</sup>2273) with the conventional three compartment cell (magnesium alloys as working electrode, a platinum foil as counter electrode and a saturated-calomel electrode (SCE) as reference electrode). Potentialdynamic polarization curves are performed over the range  $E_{ocp}(\text{open circuit potential}) \pm 300\text{mV}$ , with scanning rate 0.50mV/s. EIS are carried out over the frequency range from 100 kHz to 10 mHz with 5 mV perturbation signal at the corrosion potential.

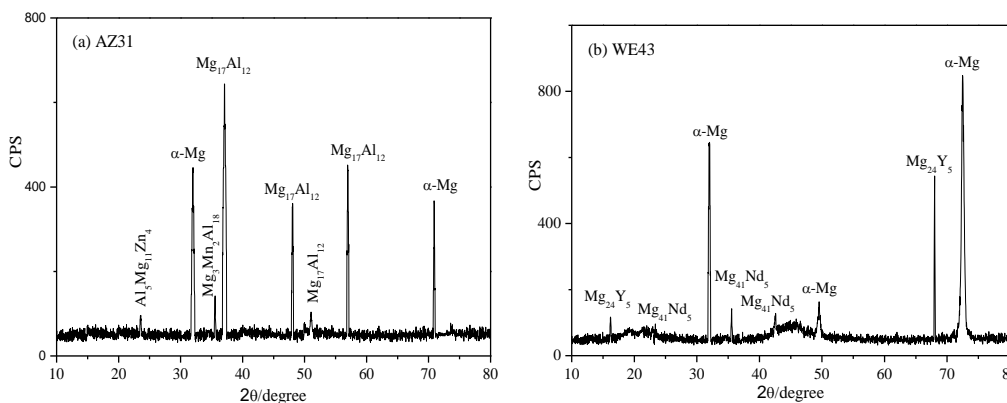
## 2.3 Corroded surface evaluation

Before and after the corrosion products are removed, each corroded surface are observed using scanning electron microscopy (SEM, SU1510, Hitachi). The composition of corrosion product is examined by X-ray diffraction (XRD, Ultima IV, Rigaku).

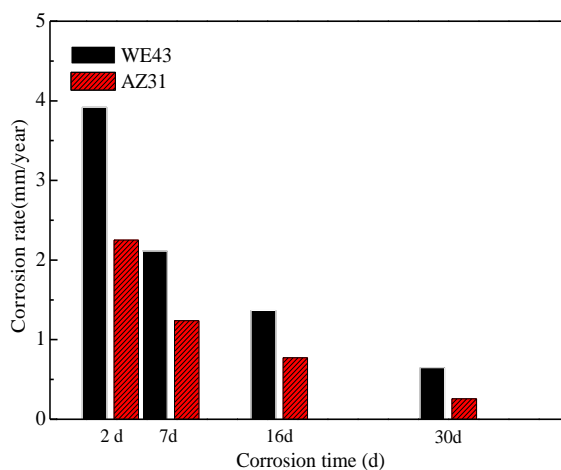
## 3. RESULTS AND DISCUSSION

Fig.1a shows the material composition of AZ31 alloy before corrosion. The as-cast AZ31 alloy mainly consists of  $\beta$  phase (Mg<sub>17</sub>Al<sub>12</sub>),  $\alpha$ -Mg, little AlMgZn and MgMnAl compounds. The  $\beta$  phase (intermetallic compounds Mg<sub>17</sub>Al<sub>12</sub>) acts as the cathode and possesses good passive behavior in broad pH range. When the anodic  $\alpha$  phase (the matrix) dissolves, the  $\beta$  phase may act as a barrier layer to inhibit corrosion [5]. The corrosion process of  $\beta$  phase is decided by its content, size and distribution.

Only high mass fraction, small grain size and continuous distributed  $\beta$  phase can deter corrosion [4]. For WE43 alloy, the XRD pattern (Fig.1b) demonstrates the existence of  $\alpha$ -Mg,  $Mg_{24}Y_5$  and  $Mg_{41}Nd_5$ . The second phase particles such as  $Mg_{12}(RE)$  and Y-rich substance have positive potential relative to magnesium matrix [11], therefore they act as sites for hydrogen evolution (cathodic reaction) in the corrosion process. In addition, rare earth element Y in WE43 alloy has the role of impurity (such as H, O, S, Cl, Fe, etc.) removing. It can change the impurities present in alloy from solute state substances to intermetallic compounds, which is benefit for corrosion resistance enhancement to some extent [12].



**Figure 1.** X-ray diffraction patterns of AZ31 alloy and WE43 alloy before corrosion



**Figure 2.** Corrosion rates of AZ31 alloy and WE43 alloy in SBF

According to results of weight loss tests in SBF, calculated corrosion rates of AZ31 alloy and WE43 alloy after immersion for 2d, 7d, 16d and 30d are shown in Fig.2. On account of the large reactive metallic surface exposed to the SBF, the initial degradation rates of two alloys are fast. Over time corrosion products formed on sample surface are thicker. Some products peel off to the container bottom, and the others adhered to matrix surface tightly which has barrier action and impeded further degradation. It is known to all that the diffusion rate of reaction species in surface products layer can affect the overall corrosion rate [14]. Tightly adhesive corrosion products made corrosion rates of two

alloys both decreased. Moreover, compared with AZ31 alloy, WE43 alloy has a relative faster dissolution rate.

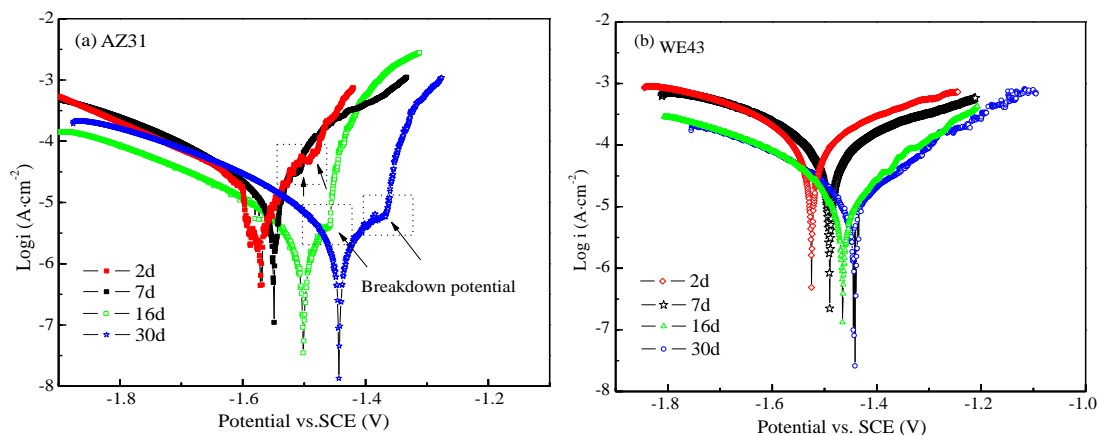


**Figure 3.** Polarization curves of AZ31 and WE43 alloys immersed in SBF

The electrochemical tests also reach the same results. The potentialdynamic polarization curves of AZ31 and WE43 alloys after exposure to SBF for 2d, 7d, 16d and 30d are shown in Fig.3. As the corrosion time increase, corrosion potentials ( $E_{cp}$ ) of these alloys both shift positively, and corrosion current densities reduce (shown in Table 3). However, polarization curves of the two different magnesium alloys have different characteristics obviously. Generally, the cathodic curves represent the reaction of hydrogen evolution, and the anodic curves are assumed to represent the magnesium dissolution [15]. On anodic polarization curve of AZ31 alloy, there are visible passivation tendency below the breakdown potential as marked on the curves. The existence of passivation tendency at the anodic sides implies the presence of oxide films on the surface of the Mg-xZn alloys [17]. The similar experimental results has been also obtained by Y. Song et al [15,17,18].

**Table 3.** Fitting results of the polarization curves

Corrosion time (d)	AZ31				WE43			
	ba (mV/decade)	bc (mV/decade)	$E_{cp}$ (V)	$I_{corr}$ ( $\mu\text{A}/\text{cm}^2$ )	ba (mV/decade)	bc (mV/decade)	$E_{cp}$ (V)	$I_{corr}$ ( $\mu\text{A}/\text{cm}^2$ )
2	112.32	-125.33	-1.57	15.85	82.36	-155.46	-1.53	125.85
7	114.46	-127.86	-1.55	10.50	85.40	-159.19	-1.49	105.32
16	119.72	-134.49	-1.50	7.94	71.24	-163.38	-1.46	62.44
30	120.82	-136.51	-1.45	6.31	74.43	-164.22	-1.44	25.10

On anodic curve of WE43 alloy, there is no distinct breakdown potential and no visible passivation tendency display on the curves. Corrosion current density ( $I_{corr}$ ) can be calculated by Tafel extrapolation [17] shown in Table 3.

The relationship of corrosion rate ( $v$ ) and  $I_{corr}$  is shown as follows:

$$v = i / zFA = I_{corr} / zF \tag{2}$$

where  $z$  is number of reaction electrons;  $F$  is faraday constant;  $A$  is electrode area. In the same reaction system,  $z$  and  $F$  are constants [18,19]. Over time, both the corrosion rates of AZ31 and WE43 alloy decrease, and the former is always lower than the latter. This result is in accord with the outcome obtained from weight loss test.

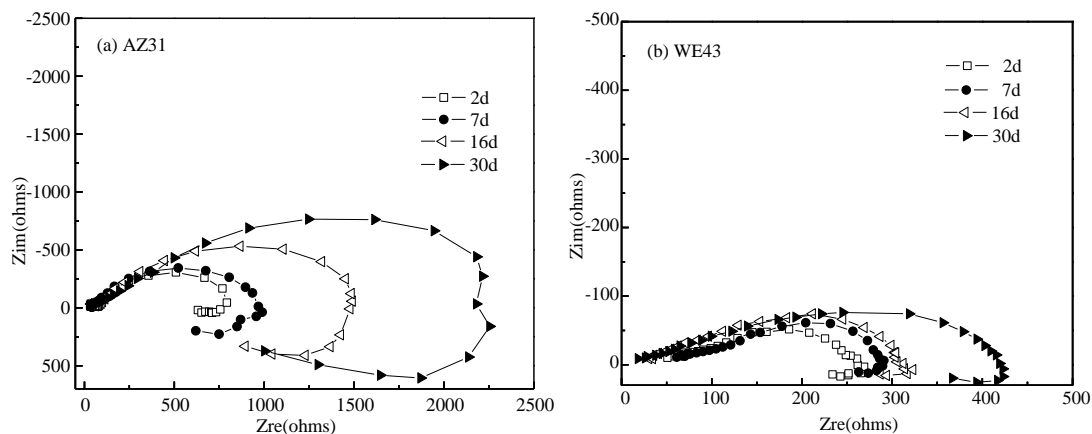
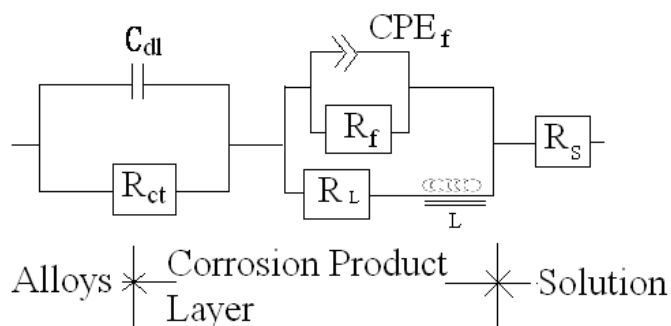


**Figure 4.** Nyquist plots of magnesium alloys immersed in SBF

Fig. 4 shows the Nyquist impedance plots of AZ31 alloy and WE43 alloy exposed to SBF for several days. The Nyquist plots consisted of one high frequency capacitance loop (corresponds to characteristics of electric double layer), one medium frequency capacitance loop (corresponds to surface film) and one low frequency inductive loop (corresponds to the partial protection of the surface oxide film)[20]. Over time there are little change on the general shape of these plots, which indicate the similar corrosion mechanism of magnesium alloys in SBF.



$R_s$ : the electrolyte resistance;  $R_{ct}$ : the charge transfer resistance;  $C_{dl}$ : the double layer capacity;  $R_f$ : the film resistance;  $CPE_f$ : the film capacity (compensate for the non-homogeneity in the system);  $R_L$  and  $L$  indicate the partial protection of the surface oxide film.

**Figure 5.** Equivalent circuit of fitting EIS data

The appropriate equivalent circuit (shown in Fig.5) is used to fit the EIS data and provides information of corrosion processes [21]. The fitting results are listed in Table 4. The charge transfer resistances  $R_{ct}$  corresponds to the dissolution of magnesium alloy and can directly characterize the corrosion resistance of the different alloys. Over time magnesium alloys corrosion make the solution composition and electrical resistivity changed, and then the charge transfer resistance  $R_{ct}$  of AZ31 alloy and WE43 alloy both increased. Compared with WE43 alloy at the same immersion time,  $R_{ct}$  value of AZ31 alloy are higher.

**Table 4.** Fitting results of the electrical elements

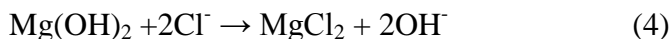
	Time (d)	$R_s$ ( $\Omega \cdot \text{cm}^2$ )	$C_{dl}$ ( $\mu\text{F} \cdot \text{cm}^{-2}$ )	$R_{ct}$ ( $\Omega \cdot \text{cm}^2$ )	CPE1-T ( $\mu\text{F} \cdot \text{cm}^{-2}$ )	n	$R_f$ ( $\Omega \cdot \text{cm}^2$ )	$R_L$ ( $\Omega \cdot \text{cm}^2$ )	L ( $\text{H} \cdot \text{cm}^{-2}$ )
AZ31	2	24.36	9.19	88.38	12.54	0.63	786.7	368.3	129.3
	7	28.94	8.80	93.23	11.17	0.67	932.2	559.4	113.9
	16	34.36	8.19	149.2	10.04	0.78	1326.7	768.5	109.3
	30	36.68	7.88	224.9	10.92	0.83	2267	1275.2	106.3
WE43	2	18.3	9.54	54.62	4.08	0.66	263.3	73.6	135.5
	7	24.77	9.24	64.33	4.95	0.77	292.7	89.7	122.9
	16	30.7	8.22	79.34	3.38	0.81	328.4	126.6	109.7
	30	31.07	7.34	109.7	3.72	0.86	387.6	153.5	84.6

The corrosion mechanism of magnesium and its alloys are generally characterized as following process [21]: (I) magnesium hydroxide film Formation. Magnesium hydroxide film will form quickly when magnesium and its alloys exposed to the test solution:



Due to the incompact properties of magnesium hydroxide film (lots of micro-holes about 10 nm in diameter on film surface), the matrix can be only partially protected [22]. Over time the fresh part of the matrix disappears, and surface products films thicken gradually.

(II) Protective  $\text{Mg}(\text{OH})_2$  films have been transformed into soluble products by aggressive ions (such as  $\text{Cl}^-$ ,  $\text{SO}_4^{2-}$ , etc.) [22]:



$\text{MgCl}_2$  is soluble and  $\text{Cl}^-$  is easy to induce pitting corrosion, therefore, the dissolution of matrix accelerates.

(III) Small irregular pieces of magnesium alloy peel off from the serious corroded matrix, which induce more fresh surface of metal exposed to test solution to be corroded.

Surface morphology of AZ31 alloy and WE43 alloy immersed in SBF after removing the corrosion products are shown in Fig.6. After corrosion for severer days, some sites of AZ31 alloy surface are covered with irregular pits. Especially, plenty of white products adhere onto the pits. For WE43 alloy, it is corroded seriously with plenty of cracks and pits on the surface. As the immersed time increase, the two alloys are all destroyed heavily and covered with much corrosion product.

Compared with AZ31 alloy, the surface of WE43 alloy is damaged seriously with much more number of large holes.

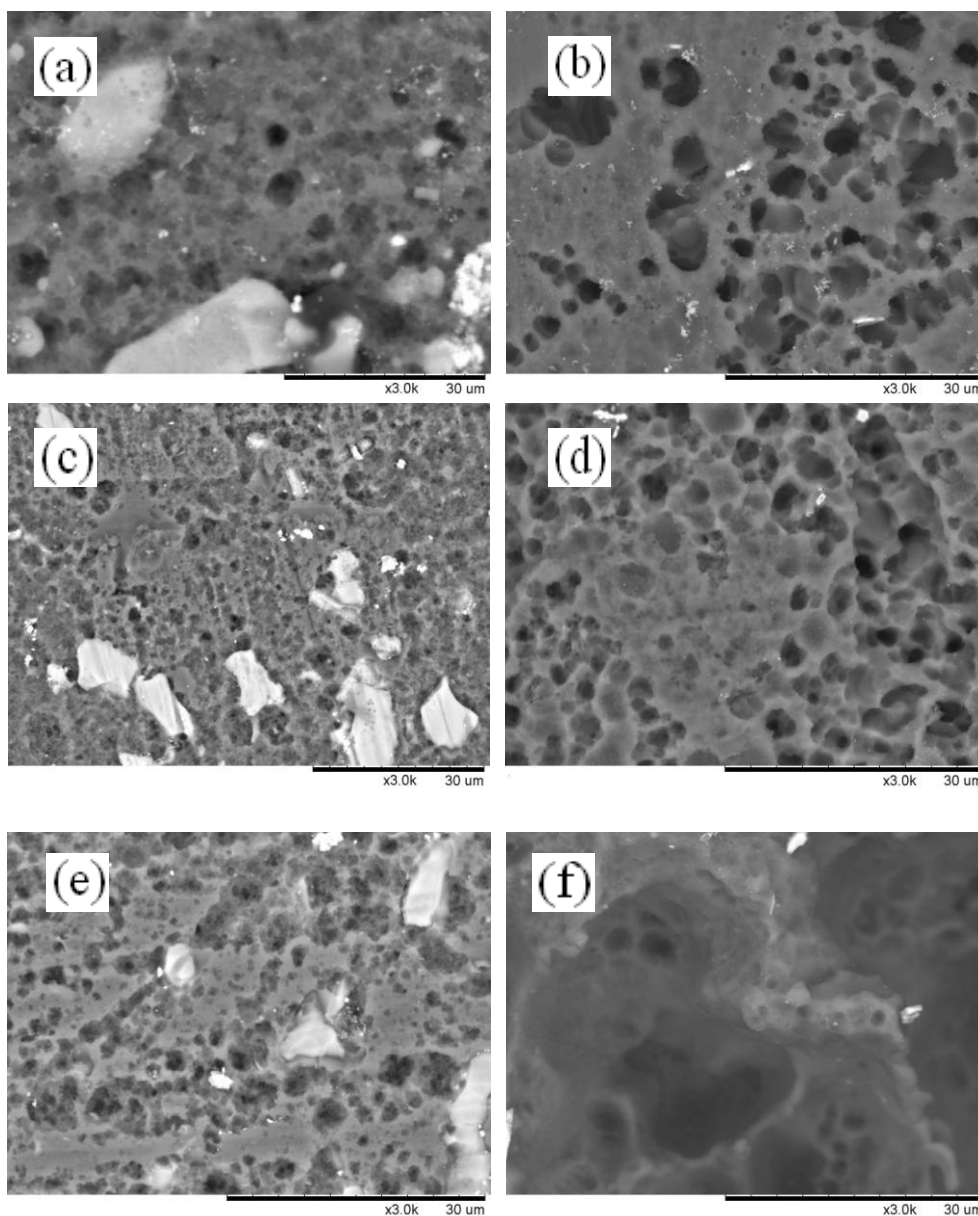


**Figure 6.** Morphology of magnesium alloys exposed to SBF for several days. AZ31 (a)7d, (c)16d, (e)30d; WE43 (b)7d, (d)16d, (f)30d

The section analysis results of these two magnesium alloys have the same conclusion. For AZ31 alloy exposed to SBF for 16 days (shown in Fig.7a), it is clear to see that the interface between corrosion product and matrix is neat, meanwhile a few shallow and narrow pits can be detected. For WE43 alloy, the interface is sinuate obviously (Fig.7b). At the same immersion time, WE43 alloy has been relatively more serious corroded.

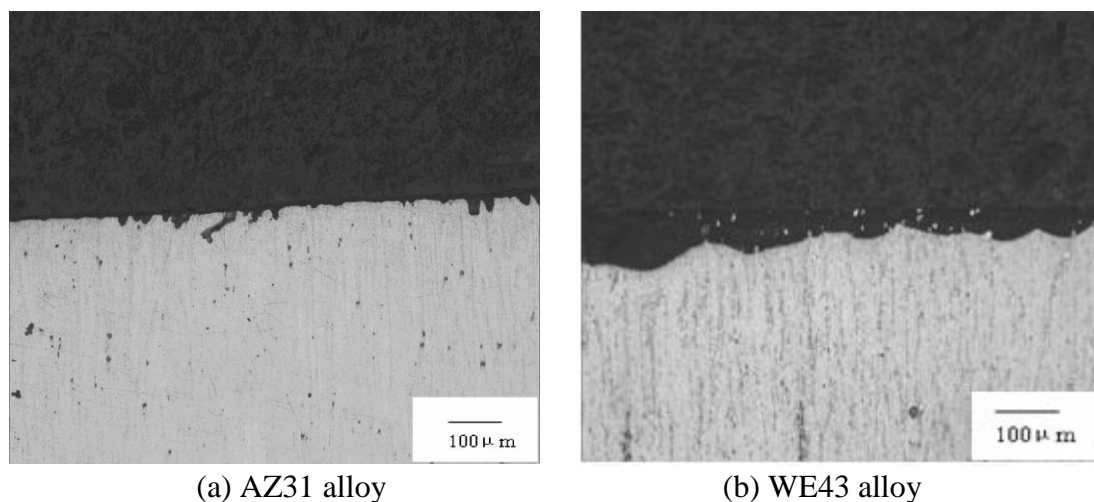


**Figure 7.** Section analysis of magnesium alloy exposed to SBF for 16 days

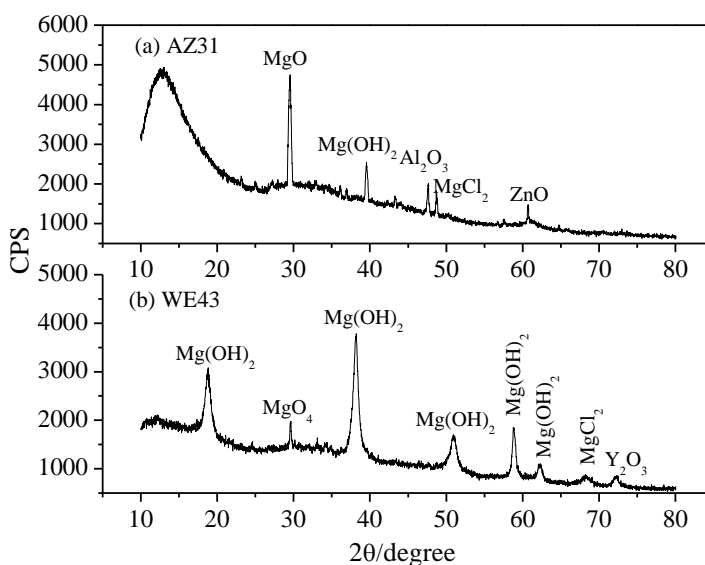


**Figure 8.** XRD analysis of corrosion products from AZ31 alloy and WE43 alloy exposed to SBF for 30 days

When weight loss test finished, the corrosion products are collected from alloy surfaces by stainless steel knife. Fig.8 shows the XRD analysis of corrosion products.  $Mg(OH)_2$  is the main corrosion products of magnesium alloys. In the corrosion products of AZ31 alloy, the oxidation products of magnesium, Al and Zn, and  $MgCl_2$  can be determined. It is reported that in humid environment, the Al components will form a continuously skeletal structure in an oxide layer of magnesium alloy. This layer has passivation properties and can hinder the corrosion of matrix more effectively than that of  $Mg(OH)_2$  and  $MgO$  layers [23-25]. For WE43 alloy,  $MgO_4$ ,  $MgCl_2$  and  $Y_2O_3$  are the main component of corrosion products. The incorporation of oxidized Y in the surface film and the Y-rich regions in matrix can both retard the biodegradation of magnesium alloys effectively[26,27].

#### 4. CONCLUSIONS

The biodegradable processes and mechanism of AZ31 alloy and WE43 alloy has been investigated in SBF. The results show that corrosion rates of AZ31 alloy and WE43 alloy immersed in SBF both decrease over time. Compared with AZ31 alloy, WE43 alloy has a faster dissolution rate. In the immersion experiment, as the time increases, some sites of AZ31 alloy surface are covered with irregular pits. The surface corrosion products are mainly consisted with the oxidation products of Mg, Al and Zn, and MgCl<sub>2</sub>. Moreover, the interface between corrosion product and matrix is relatively neat with a few shallow and narrow pits. For WE43 alloy, there are plenty of cracks and pits on the surface. MgO<sub>4</sub>, MgCl<sub>2</sub> and Y<sub>2</sub>O<sub>3</sub> are main component of corrosion products. The interface between corrosion product and matrix is sinuate ascribed to serious local corrosion happening.

#### ACKNOWLEDGEMENTS

This research was supported by the National Natural Science Foundation of China (Grant No. 51401198 and 21403194), China Postdoctoral Science Foundation (Grant No. 2014M560475) and Zhejiang province Postdoctoral Science Foundation (Grant No. BSH1402021).

#### References

1. C.Z. Yao, S.L. Tay, T.P. Zhu, H.F. Shang, W. Gao, *J. Alloys Compd.*, 645(2015)131.
2. M. Alvarez-Lopez, M. D. Pereda, J.A. del Valle, M. Fernandez-Lorenzo, M.C. Garcia-Alonso, O.A. Ruano, M.L. Escudero, *Acta Biomater.*, 6(2010)1763.
3. A. Mochizuki, H. Kaneda, *Mater. Sci. Eng. C Mater. Biol. Appl.*, 47(2015)204.
4. H.H. Elsentriecy, J. Qu, H.M. Luo, H. M. Meyer, C. Ma, M.F. Chi, *Thin Solid Films*, 568(2014)44.
5. A. Pardo, M. C. Merino, A. E. Coy, R. Arrabal, F. Viejo, E. Matykina, *Corros. Sci.*, 50(2008)823.
6. T. Cain, L. G. Bland, N. Birbilis, J. R. Scully, *Corrosion*, 70(2014)1043.
7. X. R. Long, L. Bo, L. Ling, L. Qing, *Mater. Des.*, 32(2011)4548.
8. G. L. Song, Z.Q. Xu, *Corros. Sci.*, 54(2012)97.
9. L. Wang, T. Shinohara, B. P. Zhang, *Mater. Des.*, 33(2012)345.
10. Y. Zong, G.Y. Yuan, X.B. Zhang, L. Mao, J.L. Niu, W.J. Ding, *Mater. Sci. Eng. B*, 177(2012) 395.
11. A.D. Sudholz, K. Gusieva, X.B. Chen, B.C. Muddle, M.A. Gibson, N. Birbilis, *Corros. Sci.*, 53 (2011)2277.
12. C. H. Ye, Y. F. Zheng, S. Q. Wang, T. F. Xi, Y.D. Li, *Appl. Surf. Sci.*, 258(2012)3420.
13. H. Kalb, A. Rzany, B. Hensel, *Corros. Sci.*, 57 (2012)122.
14. T.Y. Nguyen, A.F. Cipriano, R.G. Guan, Z.Y. Zhao, H.N. Liu, *J. Bioned. Mater. Res. A*, 103(2015)2974.
15. Y.W. Song, E.H. Han, D.Y. Shan, C.D. Yim, B.S. You, *Corros. Sci.*, 60(2012) 238.
16. Standard Practice for Laboratory Immersion Corrosion Testing of Metals, 2004, 1.
17. Y.W. Song, E.H. Han, D.Y. Shan, C.D. Yim, B.S. You. *Corros. Sci.*, 65(2012) 322.
18. Y. W. Song, D. Shan, R. Chen, F. Zhang, E.H. Han, *Mater. Sci. Eng. C.*, 29(2009) 1039.
19. A. Pardo, M.C. Merino, A.E. Coy, R. Arrabal, F. Viejo, E. Matykina, *Corros. Sci.*, 50(2008)823.
20. A.C. Hännzi, P. Gunde, M. Schinhammer, P.J. Uggowitzer, *Acta Biomater.*, 5(2009)162.
21. J.Q. Zhang, *Electrochemical Measurement Technology*, Beijing: Chemical Industry Impress, 2010, 29.
22. W.H. Jin, G.S. Wu, H.Q. Feng, W.H. Wang, X.M. Zhang, P.K. Chu. *Corros. Sci.*, 94(2015)142.

23. L. Bukovinová, B. Hadzima, *Corros. Eng. Sci. Techn.*, 47(2012)352.
24. M. Jamesh, G. Wu, Y. Zhao, P. K. Chu. *Corros. Sci.*, 69(2013)158.
25. G.R. Argade, K. Kandasamy, S.K. Panigrahi, R.S. Mishra. *Corros. Sci.*, 58(2012)321.
26. G. Wu, Y. Zhao, X. Zhang, M.I. Jamesh, P.K. Chu, *Corros. Sci.*, 68(2013)279.
27. M. Jamesh, S. Kumar, T.S.N. Narayanan, *J. Coat. Technol. Res.*, 9(2012)495.

© 2015 The Authors. Published by ESG ([www.electrochemsci.org](http://www.electrochemsci.org)). This article is an open access article distributed under the terms and conditions of the Creative Commons Attribution license (<http://creativecommons.org/licenses/by/4.0/>).